A New 2,2,2-Trifluoroethanol Model for Molecular Dynamics Simulations

Marco Fioroni[†] and Klaus Burger[†]

Fakultat fur Chemie und Mineralogie Institut fur Organische Chemie Johannisallee, 29, 04103 Leipzig, Germany

Alan E. Mark and Danilo Roccatano*

Groningen Biomolecular Sciences and Biotechnology Institute (GBB), Department of Biophysical Chemistry, University of Groningen, Nijenborgh 4, 9747 AG Groningen, The Netherlands

Received: June 12, 2000; In Final Form: October 16, 2000

A new model for 2,2,2-trifluoroethanol is proposed. It is a 7-atom model with the methylene group treated as an united atom. The model was optimized to reproduce the physicochemical properties of the pure liquid. The properties of the new model were compared with the available experimental data over a range of temperatures. Furthermore, mixtures with the SPC water model were simulated to assess the ability to reproduce available thermodynamic and kinetic data as well as dielectric properties. The model provides a good agreement with experimental data for the neat liquid and for mixtures with water.

I. Introduction

2,2,2-Trifluoroethanol (TFE) is an important cosolvent in the study of protein and peptide structure. Its effect on the structure of these molecules has been studied for many years and the mechanism by which TFE promotes the stabilization of particular secondary structure elements is beginning to be understood.[1] However, despite the large amount of experimental data available, the use of this solvent in molecular dynamics (MD) simulation studies of biomolecular system is restricted to just a few examples.[2−4] One reason for this is the lack of a reliable TFE model for these simulations. Models of TFE used up until now have been poorly characterized. No systematic study of the extent to which a given TFE model reproduces the physicochemical properties of bulk TFE or TFE water mixtures has to our knowledge been published. In this study we have parametrized a new model for TFE consistent with the GROMOS96[5] force field for biomolecular simulations. Nonbonded interactions are described using Lennard-Jones and Coulomb terms. Polarizability, which is important for the correct reproduction of the physicochemical properties of the molecule, is incorporated implicitly into the assigned partial charges. We have compared the properties of our model with the available experimental data. The physicochemical properties used to validate the model in the pure liquid state include the density, pressure, evaporation enthalpy, static dielectric constant, shear viscosity, heat capacity, and diffusion constants.

We have also studied the physicochemical and structural properties of water−TFE mixtures. These systems have broad application in the study of the stabilization of secondary structures in peptides and proteins.[1] Although the mechanism by which TFE stabilizes secondary structures is not completely understood, there is experimental evidence to suggest that not only the low dielectric constant and hydrogen-bonding effects are important but also the capability of TFE to form clusters in aqueous solution.[6] Recent studies with small-angle X-ray scattering (SAXS),[6] NMR, and FTIR[7] have provided evidence of microheterogeneity in TFE−water solutions. According to these studies, cluster formation reaches a maximum at a concentration of around 30% TFE, the optimal concentration to induce secondary structure stabilization in peptide and proteins.

In section II the procedure for the optimization of the TFE interaction function parameters is described and the computational procedure used to perform the MD simulations is reported. In section III the structural and physicochemical properties of pure TFE and in section IV of the mixture with water are presented. Finally, section V contains a summary and conclusions.

II. Method

A. TFE Force Field Parameters. Most bulk liquid properties are relatively insensitive to the intramolecular force field parameters. For this reason, bond lengths (considered as rigid constraints) and bond angles values were taken from existing TFE models.[2,3] The hydrogens and the carbon of the methylene group were considered as a single united atom. This approximation was used as the benefit in terms of additional model parameters (the presence of the explicit hydrogens) did not justify the increased computational cost.

The initial point charge distribution was estimated based on ab initio calculations. Geometry optimizations at SCF level were carried out using a 6-31G(p,d) basis set which includes polarization functions. The single-point energies were calculated on the optimized structures including electronic correlations at the MP2 level. Partial atomic charges were calculated, at the RHF and MP2 level, using electrostatic potential fits to the charge density of the optimized conformer. The CHELPG procedure[8] was used to perform the electrostatic potential fits as this has been shown to give reliable partial charges for use

* Corresponding author. Fax: +31-50-3634800. E-mail: roccata@chem.rug.nl.
† Fax: +49-341-9736599.

10.1021/jp002115v CCC: $19.00
Published on Web 12/02/2000

TABLE 1: Summary of the Geometric Parameters Obtained from the Different Quantum-Mechanical Calculations for TFE in Vacuo

	Gg		
	calc	exp[a]	Gt calc
$r(C-F_1)$	0.1329	0.1343	0.1318
$r(C-F_2)$	0.1317	0.1343	0.1319
$r(C-F_3)$	0.1323	0.1243	0.1327
$r(C-C)$	0.1510	0.1490	0.1508
$r(C-O)$	0.1386	0.1430	0.1388
$r(O-H)$	0.0944		0.0942
$r(H\cdots F)$	0.2520	0.256	
$\theta(F_1-C-F_2)$	107.44		107.88
$\theta(F_1-C-F_3)$	107.66		107.68
$\theta(F_2-C-F_3)$	107.90		107.68
$\theta(F_1-C-C)$	110.60	110.44	112.06
$\theta(F_2-C-C)$	112.56	111.87	112.02
$\theta(F_3-C-C)$	110.50	110.44	109.32
$\theta(C-C-O)$	111.34	112.30	107.83
$\theta(C-O-H)$	110.09	105.40	110.26
$\theta(O-H\cdots F)$			
$\phi(O-C-C-F_1)$	58.20	60.23	60.65
$\phi(O-C-C-F_2)$	−61.98	−60.23	−60.76
$\phi(O-C-C-F_3)$	−182.69	−180.00	179.96
$\phi(H-O-C-C)$	−66.40	−68.97	−180.00

[a] Values taken from ref 11.

in molecular dynamics or Monte Carlo force fields.[9] All ab initio calculations were performed using the GAUSSIAN94 package.[10]

The conformations examined were the Gauche:gauche (Gg) and the Gauche:trans (Gt) where the first letter refers to the conformation about the C−C bond ($\phi(O-C-C-F_1) = 60°$) and the second is the conformation about the C−O bond ($\phi(H-O-C-C) = -60°$ for g and −180° for t conformers). In Table 1 the geometric characteristics of the optimized structures are reported. The calculated Gg conformation has the hydroxy hydrogen in the gauche position with respect to the CF_3 group, forming an intramolecular hydrogen bond with one of the fluorine atoms. The internal hydrogen bond is characterized by a H···F bond distance of 2.52 Å. This is in good agreement with the value of 2.56 Å obtained from experimental microwave spectroscopy measurements.[11] Thus, there is overall agreement between the calculated and observed Gg conformer, considering the experimental uncertainties. Bonds and angles show only small variations upon rotation to the Gt conformer. The difference in energy (MP2 level) between the two conformers is 9.9 kJ/mol with the Gg conformer the lower in energy. These values are in close agreement with the experimental value (13.8 kJ/mol) obtained from spectroscopic measurements in chloroform solution.[12] The Gt conformer is destabilized by repulsion between the oxygen and halogen lone pair electrons.[13] This effect is not reproduced by the nonbonded interactions in our model, and the Gt and the Gg conformers are approximately degenerate in vacuum. The use of dihedral potential functions to fit the potential energy surface obtained from ab initio calculation, prevented the simultaneous reproduction of both thermodynamic and dynamical liquid properties. The stabilization of the Gg with respect the Gt form using additional dihedral potentials reduced drastically the mobility of molecules. For this reason our model has no dihedral potential functions on FCCO angle and a standard cosine potential function with a small barrier on the CCOH dihedral. The last function was found necessary to refine the agreement of the bulk properties with the experimental data. Therefore, the model does not reproduce the difference in energy between the Gg and Gt conformer obtained from in vacuum ab initio calculations. The model was optimized to reproduce the liquid properties of TFE. We note there is no experimental evidence shows a predominance of gauche form with respect the trans form in this phase.

TABLE 2: Summary of the Quantum-Mechanical Charge Calculations of TFE in Vacuo (Charges in electrons and Dipoles in debyes)

	RHF (Gg)	MP2 (Gg)	RHF (Gt)	MP2 (Gt)	Gg-Gt (MP2)
C	0.559	0.415	0.713	0.547	−0.132
F	−0.203	−0.159	−0.219	−0.168	0.009
F	−0.197	−0.150	−0.219	−0.168	0.018
F	−0.228	−0.180	−0.270	−0.215	0.035
C	0.141	0.135	0.126	0.122	0.013
H	0.037	0.029	0.042	0.035	0.006
H	0.097	0.093	0.042	0.035	0.058
O	−0.628	−0.593	−0.673	−0.624	0.031
H	0.421	0.409	0.459	0.436	−0.027
dipole[a]	1.874	1.635	3.530	3.136	

[a] Experimental value equal to 2.09.[31]

In Table 2 the calculated charges are reported together with the dipole moments. In the last column of Table 2, the differences between the partial charges, obtained from a MP2 calculation, of the Gg and Gt conformer atoms, are reported. The largest deviation occurs at the trifluoromethyl carbon atom, with a variation of −0.132 ue. As the hydrogens on the methylene carbon atom were not treated explicitly in the final model the charges on hydrogens obtained from calculations were added to the carbon.

Initial estimates for the Lennard-Jones (LJ) parameters were taken from the GROMOS96[5] force field while an initial set of charges were obtained from MP2 calculations on the optimized Gg conformer. The choice of this set of charges is motivated by experimental evidence of the larger abundance[11,14] of the Gg conformer in gas phase; however, as shown above, the differences among quantum mechanically calculated charges in the two conformers are quite small. Starting from this set of nonbonded parameters, the model was systematically optimized primarily by modifying the partial charges of all atoms and by modifying the fluorine LJ parameters. The LJ interaction parameters between two different atom types were calculated as geometric means of the corresponding LJ parameters of the atom types, i.e., $C^{\alpha}_{1,2} = \sqrt{C^{\alpha}_{1,1} C^{\alpha}_{2,2}}$ (with $\alpha = 12$ or 6) is the LJ parameters for the interaction between atoms 1 and 2 where $C^{\alpha}_{1,1}$ refers to the interaction of atom 1 with itself.

In vacuo simulations at room temperature, the Gg conformation adopted by the model is characterized by $\phi(H-O-C-C) = 72°$, $\phi(F_1-C-C-O) = 62°$, and $r(H\cdots F) = 0.264$ nm.

The parameter optimization was performed adjusting the LJ parameters for the fluorine atom and the partial charges, obtained from QM calculations, of the different atoms, to reproduce densities and enthalpies of vaporization at 293, 298, and 313 K and the tracer diffusion coefficient at 298 K. Details of the systems used for the simulations are reported in the next section. The final optimized TFE parameters are reported in Table 3.

B. MD Simulations. Different MD simulations of neat TFE and of mixtures of TFE with SPC water were performed. In Table 4 the simulation parameters of the different pure TFE systems are summarized. The systems were simulated at three different temperatures, 293, 298, and 313 K, using two different cubic boxes, with the length of the box edge being approximately 3 and 4 nm, respectively, and periodic boundary conditions (PBC). Simulations were performed at constant density and at constant pressure. The different system sizes were used to analyze the effect of the box size on the physicochemical properties of the pure solvent. In the case of the mixtures, five different NPT simulations at 298 K were performed. All the

TABLE 3: Parameters for the TFE Force Field

atoms	$C^6_{1,1}$/(kJ mol^{-1} nm^6) × 10^3	$C^{12}_{1,1}$/(kJ mol^{-1} nm^{22}) × 10^6	q/e
F	1.177862	1.000000	−0.17
C	2.340624	3.374569	0.452
CH2	7.104804	25.775929	0.273
O	2.261954	1.505529	−0.625
H	0.0	0.0	0.410

bond	distance(nm)
F−C	1.36
CH2−O	1.43
CH2−C	1.53
O−H	1.00

bond angle	θ_0 (deg)	K_θ/kJ mol^{-1} rad^{-2}
H−O−CH2	109.5	397.5
O−CH2−C	110.3	460.2
CH2−C−F	111.4	460.2
F−C−F	107.6	460.2

dihedral	ϕ_0 (degrees)	K$_\theta$/kJ mol^{-1} rad^{-2}
H−O−C−C	3	1.300

TABLE 4: Summary of Simulations of the Pure TFE[a]

T (K)	conditions	N_{TFE}	ρ (kg/m^3)	P (bar)	ΔH_{vap} (kJ mol^{-1})
293	NVT	536	1.391	−1.2	43.2
293	NPT	536	1.390	1.0	43.3
298	NVT	526	1.383	1.3	42.6
298	NPT	526	1.383	1.0	42.7
313	NVT	526	1.356	2.2	40.5
313	NPT	526	1.358	1.0	40.6
		Experiment[b]			
293	NPT		1.391	1.0	43.8
298	NPT		1.383	1.0	42.9
313	NPT		1.356	1.0	40.5

[a] The standard deviations of computed values are 0.01 kg/m^3, 100 bar, and 0.4 kJ/mol for density, pressure, and vaporization enthalpy, respectively. [b] Values taken from ref 46.

TABLE 5: Thermodynamic and Dynamical Properties of Pure TFE (Experimental Values in Parentheses)

T (K)	$\beta_T \times 10^4$ [a]	$\alpha \times 10^3$ [b]	C_P[c]	$D \times 10^6$ [d]	$\eta \times 10^3$ [e]	ϵ_r [f]
293	1.36 (1.34)	1.20	204	0.3	2.30 (2.00)	
298	1.38 (1.22)	(1.19)	(177.8)	0.4 (0.6)	1.95 (1.75)	17.6 (26.7)
313	1.44 (1.15)	1.21	209	0.6	1.52 (1.22)	

[a] In bar^{-1}. [b] In K^{-1}. [c] In J/K. [d] In cm^2 s^{-1}. [e] In kg m/s^2. [f] In debyes.

simulations were run for 2 ns after the equilibration. The mixture containing 34% TFE was simulated for 10 ns to check for possible phase separation. In Table 5 a summary of these simulations is reported.

In all simulations the temperature was maintained close to the intended values by weak coupling to an external temperature bath[15] with a coupling constant of 0.1 ps, and the pressure by weak coupling to an external pressure of $P_0 = 1$ bar with a coupling constant of $\tau_P = 4$ ps.[15] In the constant pressure simulations, the parameter corresponding to the isothermal compressibility of liquid TFE was set to its experimental value (1.22×10^{-4} kJ^{-1} mol nm^3) at 298 K.[16] The simple point charge (SPC)[17] water model was used in the simulations of TFE and water. The LINCS algorithm[18] was used to constrain all bond lengths in TFE. For the water molecules the SETTLE algorithm[19] was used. A relative dielectric permittivity, $\epsilon_r = 1$, and a time step of 2 fs were used. A twin range cutoff was used for the calculation of the nonbonded interactions. The short-range cutoff radius was set to 0.8 nm and the long-range cutoff radius to 1.4 nm for both Coulombic and Lennard-Jones interactions. The cutoff values are the same as those used for the GROMOS96 force field parametrization.[5] Interactions within the short-range cutoff were updated every step whereas interactions within the long-range cutoff were updated every 5 steps together with the pairlist. To initialize the simulations, the systems were first minimized using the steepest descent algorithm. Then initial velocities, obtained from Maxwellian distributions at the desired initial temperatures, were assigned to all atoms. Runs of 100 ps were performed to relax and equilibrate the systems.

Thermodynamic properties, such as the heat capacity, the isothermal compressibility, and the thermal expansion coefficient, can be obtained from the second moment of the central distribution of an appropriate thermodynamic variable,[20] or from two simulations of the system at different thermodynamic states. In the first case, there are two main problems that have to be considered. One is the reliability of the method used to generate the simulated ensemble; the weak coupling method used for our simulations does not exactly reproduce a canonical ensemble.[21] The other problem is the slow convergence of the second moments. Very long simulations are required to obtain good sampling. In contrast, the first moment (mean) is less dependent on the method used in the simulation to generate the statistical ensemble, and, furthermore, the convergence to the equilibrium value is fast. For these reasons, we have in general calculated thermodynamic properties using numerical derivatives. In the case of the heat capacity, values obtained from fluctuations of the potential energy are also reported. In this case we have used a recent derivation[21] of the fluctuation equation to calculate heat capacity in NVT ensemble that makes a correction to the energy fluctuations obtained from the weak coupling method to obtain the correct canonical ensemble.[21] The dielectric constant was estimated from the fluctuation of the total dipolar moment, however; to obtain convergence, longer trajectories for this calculation were performed.

The standard deviations of equilibrium properties were estimated using the block averaging method as described previously.[20,22] All simulations and analysis were performed using the GROMACS software package[23] in double precision.

III. Physicochemical Properties of Pure TFE

A. Structural Properties. The intermolecular radial distribution functions (RDFs), denoted by $g_{xy}(r)$ and calculated from the simulations[20] at different temperatures, for the pairs F−H and O−H are shown in Figure 1. In the same figure the running integration number (RIN)

$$n_{xy} = 4\pi\rho_0 \int_0^R g_{xy}(r') r'^2 \, dr' \qquad (1)$$

where ρ_0 is the number density of the atoms of kind y, are reported. The RIN gives the average number of atoms y contained in a sphere of radius R centered on atom x.

The $g(r)$ between oxygen and hydrogen gives a first peak at 0.168 nm with a RIN equal to one. The sharp peak indicates the presence of strong specific H-bond interactions. A second coordination shell peak is at 0.33 nm. The coordination number calculated up to the second minima (0.45 nm) is 3.5 H atoms. The $g(r)$ functions for the F−H pair do not have a well-defined first peak. At the distance for a possible H···F bond there is a rise in the $g(r)$ curve and the first indication of an organized shell is a shoulder at 0.32 nm. The first defined peaks are at 0.38 and 0.43 nm. The first peaks for the F−O and O−O $g(r)$'s (not shown) are at 0.29 and 0.26 nm, respectively. The values

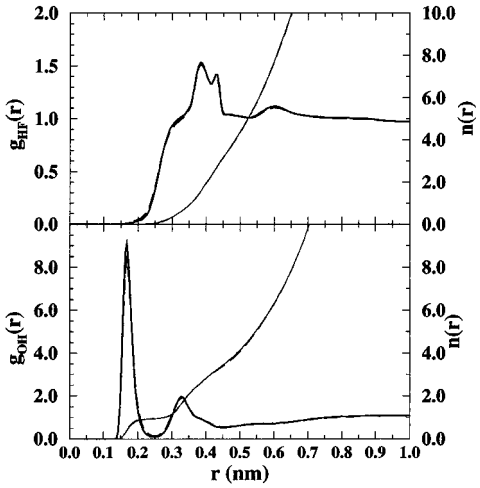

Figure 1. Pair distribution functions derived from MD simulations for F−H (upper panel), O−H (lower panel) at 293 K (long dashed line) and 313 K (solid line). The thin lines are the corresponding integral of the number of atoms.

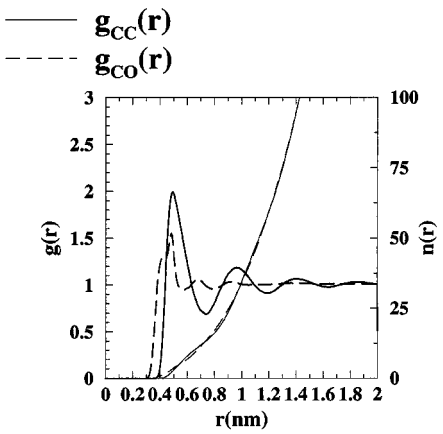

Figure 2. C−C (solid line) and C−O (dashed line) pair distribution functions as derived from MD simulations at 298 K. The thin lines show the running integration numbers.

of the distances are close to those found by Curtiss et al.[24] who proposed based on experimental measurements and theoretical calculations of vapor phase that TFE was possibly dimeric in the vapor phase.

The $g_{CC}(r)$ and $g_{CO}(r)$ are reported in Figure 2. The oscillating behavior of the $g_{CC}(r)$, indicates the presence of long-range structural order. The overlapped C−O function has an internal contribution, defined by the shoulder and the first peak at 0.42 and 0.48 nm, respectively, and a rapid decreasing part, corresponding to the intermolecular contribution. A snapshot from the trajectory showing the spatial arrangement of TFE molecules is displayed in Figure 3. In this figure hydrogen bonds are indicated by the broken lines. A hydrogen bond was considered to exist if the distance O···H is less than 0.25 nm, and the angle O−H···O greater than 60°. The average number of hydrogen bonds per molecule of TFE at 293, 298, and 313 K was ≈2 (considering oxygen as donor and acceptor) in all cases. The TFE molecules appear connected by a "web" of intermolecular hydrogen bonds. There is a small tendency for the more hydrophobic CF_3 parts to cluster. The F···H hydrogen bond seems not to play an important role in the liquid. Despite some evidence of long-range order, TFE does not adopt a stable micellar like structure. X-ray scattering data on the pure liquid[25] indicates the presence of intramolecular hydrogen bonds (corresponding to the gauche conformer) or the presence of small clusters containing a few molecules of TFE, as we have found in the simulations.

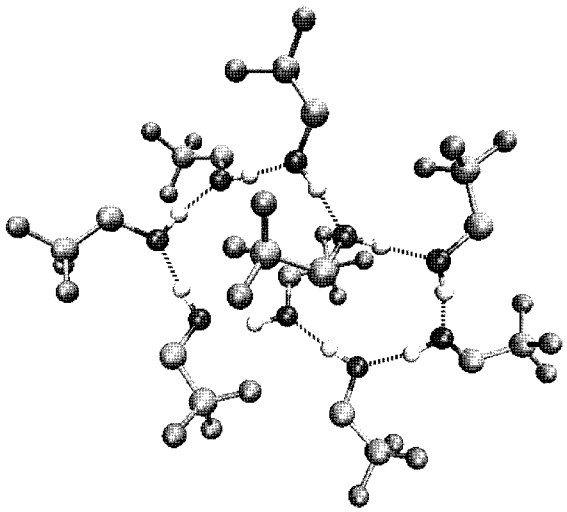

Figure 3. Example of a typical TFE cluster from the pure TFE simulation. The dotted lines are the H-bonds interactions.

B. Thermodynamic Properties. Different thermodynamic properties of liquid TFE have been used to optimize the new model and to control its capability to reproduce experimental properties. The thermodynamic properties used for the optimization were the density and the enthalpy of vaporization at three different temperatures. The other properties calculated were used as controls. In Tables 4 and 5, a summary of the calculated properties along with the experimental values, where available, are reported. The experimental density and pressure for TFE at a given temperature were taken from ref 16 and have an estimated error of 0.1%. The density ρ is within 0.1% of the experimental value at 1 bar for a range of temperature from 293 to 313 K. As with other solvent models, the pressure at constant volume is very sensitive to the method used for the calculation of long-range interactions.[27] Reducing the long-range cutoff radius from 1.4 to 1.2 nm, results in an increase in the average pressure of ≈100 bar. Other properties remain almost unaffected.

A strong dependence on the system size was noted when calculating the pressure and density. Small boxes are influenced by PBC and longer simulations are necessary to achieved a good convergence. For example, in the simulation at the lowest temperature (293 K), with a box containing 226 TFE molecules under NVT conditions, the pressure was anisotropic (the diagonal elements of tensor pressure were 32, 50, and 3.2 bar, respectively) and the density in NPT conditions deviated by up to 0.26%. Furthermore, the total average dipole moment of the box was also anisotropic denoting the presence of molecular order induced by the PBC. These effects disappeared when the temperature was greater than 298 K or the length of the box edges greater than 3 nm.

The heat of vaporization was estimated as

$$\Delta H_{vap} = [E_{inter}(g) - E_{inter}(l)] + [E_{intra}(g) - E_{intra}(l)] + RT \quad (2)$$

where E_{inter} is the total potential energy for the intermolecular nonbonded interactions and E_{intra} is the intramolecular energy (angles, torsions, intramolecular nonbonded interactions). $E_{inter}(g)$ was assumed to be zero while the $E_{intra}(g)$ was determined from an average of MD simulations of the isolated molecule.

The model reproduces the ΔH_{vap} at the different temperatures tested to within the experimental error.

The isothermal compressibility β_T was estimated using a finite difference derivative of the form

$$\beta_T = -\frac{1}{V}\left(\frac{\delta V}{\delta P}\right)_T = \frac{1}{\rho}\left(\frac{\delta \rho}{\delta P}\right)_T = \left(\frac{\delta \ln \rho}{\delta P}\right)_T \approx \left(\frac{\ln(\rho_2/\rho_1)}{P_2 - P_1}\right)_T \quad (3)$$

where ρ_1, ρ_2 and P_1, P_2 are densities and pressures obtained from two simulations at the same temperature but at different pressures. The difference in pressure was achieved by a small reduction (0.5%) in the volume of the simulation boxes. This variation produced an increase of pressure of 40 bar.

The values obtained were 1.36×10^{-4}, 1.38×10^{-4}, and 1.44×10^{-4} bar^{-1}, at 293, 298, and 313 K, respectively. These are in reasonable agreement with the experimental[16] values of 1.15×10^{-4}, 1.22×10^{-4}, and 1.34×10^{-4} bar^{-1}, at 293, 298, and 313 K, respectively.

The thermal expansion coefficient was evaluated as

$$\alpha = \frac{1}{V}\left(\frac{\delta V}{\delta T}\right)_P \approx -\left(\frac{\ln(\rho_2/\rho_1)}{T_2 - T_1}\right)_P \quad (4)$$

The values α were calculated in the ranges 293−298 K and 298−313 K. The calculated values in these ranges were 1.20×10^{-3} and 1.21×10^{-3} K^{-1}, respectively. The agreement with the experimental one of 1.19×10^{-3} K^{-1} at 298 K is good.

The constant volume heat capacity was obtained as numerical derivative, using the following equation:

$$C_V = \left(\frac{\delta E}{\delta T}\right)_V \approx \left(\frac{U_2 - U_1}{T_2 - T_1}\right)_V + 7.5R + C_V^{vib} \quad (5)$$

or from the fluctuations of the potential energy by[21]

$$C_V = \left(\frac{R\langle(\delta U)^2\rangle}{N(RT)^2 - \frac{2\alpha\langle(\delta U)^2\rangle}{3N}}\right)_T + 7.5R + C_V^{vib} \quad (6)$$

where E is the average total energy, U the average potential energy per mole of molecules, δU the fluctuation of the potential energy, R the universal gas constant, and N the number of molecules in the simulation box. The parameter α is defined by[21] $\alpha = \sqrt{(\langle(\delta K)^2\rangle/\langle(\delta U)^2\rangle)}$, where δK is the fluctuation of the kinetic energy. C_V^{vib} is a correction term for the vibrational contribution to the heat capacity from the constrained and/or missing degree of freedom (bonds). This value was estimated from the partition function for a harmonic quantum mechanical oscillator using experimental normal-mode frequencies.[28] The fundamental modes were obtained from the experimental IR data reported by Pettilla[29] and Kalasinsky.[30] The fundamental frequencies for vibrations of CH_2 group hydrogens and the stretching modes of the constrained bonds were used. In this way a value of $C_V^{vib} \approx 10$ J/K (at 298 K) was estimated.

From the C_V it is possible to calculate the constant pressure heat capacity using the expression:

$$C_P - C_V = T\frac{v\alpha^2}{\beta_T} \quad (7)$$

where v is the molar volume, á the thermal expansion coefficient and β_T the isothermal compressibility. The correction term was calculated using values obtained from the simulations. The value of the difference at 298 is 0.004 J/K. The value of C_p calculated from the simulations at 293 and 298 K, using the relations 5 and 7, is 204 J/K. The values calculated from simulations at 298 and 313 K is 209 J/K. The C_p experimental value at 298 K is 177.8 J/K.[31] Using eq 6, we obtained values for C_p equal at 149, 148, and 140 J/K at 293, 298, and 313 K, respectively.

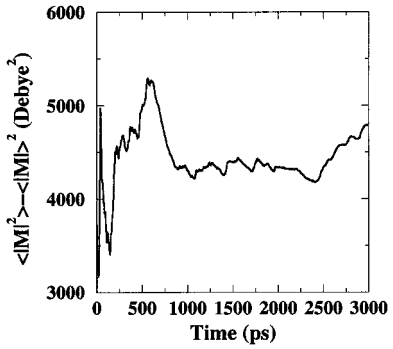

Figure 4. Cumulative average of the total dipole moment fluctuation as a function of time obtained from the 298 K simulation with reaction field.

C. Dynamical Properties. The tracer diffusion coefficient (D) at 298 K was another property used to optimize the parameters of the model. The values of D at 293 and 313 K and the other calculated kinetic properties were used as controls.

Tracer Diffusion Coefficients. The tracer diffusion coefficients (D) were calculated using the Einstein relation[20] from the slope of the center of mass mean square displacement (msd) of TFE molecules. The msd was calculated for each TFE molecule in the simulation box. Multiple starting points (each every 75 ps) were used to evaluate the msd curve. The use of well-separated starting points improves the statistics of the curve and reduces the effects of correlations on the computed value of D.[20] The resulting average msd curve was used to estimate the slope by linear regression. In the regression, the first 5 ps of the msd curve, which contains the collisional part of the diffusion curve, was neglected. The D values were computed at 293 , 298 , and 313 K and compared with the experimental values at 298 K.[7] The experimentally determined diffusion coefficient for pure TFE at 298 K is 0.6×10^6 cm^2 s^{-1}.[7] The calculated values are 0.3×10^6, 0.4×10^6, 0.6×10^6 cm^2 s^{-1}, for 293, 298, and 313 K, respectively.

Static Relative Permittivity. The static relative permittivity ϵ_r of liquid TFE has been calculated from the fluctuation in the total dipole moment $\langle M^2\rangle$ of the system using the equation[32]

$$(\epsilon_r - 1)\left(\frac{2\epsilon_{RF} + 1}{2\epsilon_{RF} + \epsilon_r}\right) = \frac{\langle M^2\rangle - \langle M\rangle^2}{3\epsilon_0 V k_B T} \quad (8)$$

where ϵ_{RF} is the relative permittivity used in the reaction field treatment, V the volume, k_B the Boltzmann constant, and T the temperature. Since the fluctuation of $\langle M^2\rangle$ converges very slowly, a simulation of 3 ns at 298 K was performed using a reaction field in the treatment of the electrostatic interactions. In Figure 4 the cumulative average of the total dipole moment fluctuation of the system is reported as a function of time. The final value for ϵ_r is 17.6 D. This is smaller than the experimental value (26.7 D at 298 K).[33] The effect of ϵ_{RF} on the ϵ_r value was tested by performing different simulations with slightly different values of ϵ_{RF} in the range 17−37 D. The resulting ϵ_r vralues do not vary significantly.

Shear Viscosity. Shear viscosities were calculated at 293, 298, and 313 K using the method described by Berendsen.[34,35] In this method the viscosity of the liquid is estimated from

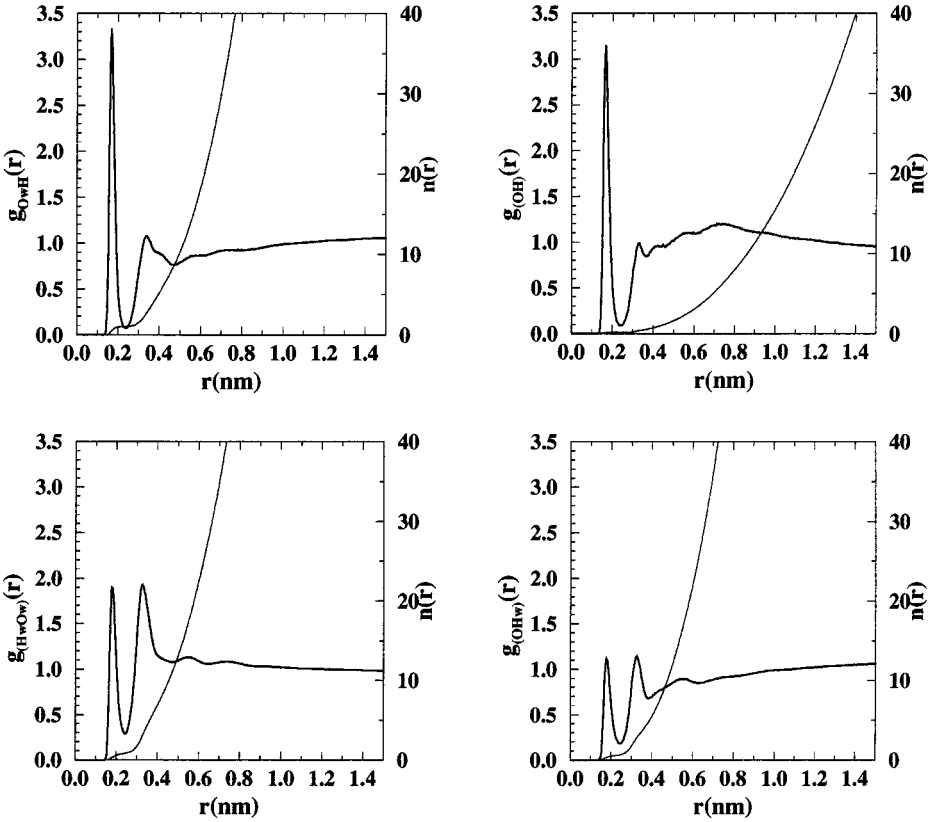

Figure 5. Hw-Ow, H−Ow, O−Hw, and O−H pair distribution functions for the 34% mixture. The thin lines show the running integration numbers.

nonequilibrium simulations where an external shear-stress acceleration field:

$$a_{i,x} = A \cos\left(\frac{2\pi z_i}{l_z}\right) \tag{9}$$

with $a_{i,x}$ being the acceleration in the x direction, A the acceleration amplitude, z_i the z-coordinate of the particle, l_z the length of the box in the z-direction, is applied to the system. The external acceleration field induces a velocity gradient of the same shape. Under these conditions, for a classical (Newtonian) fluid, the dynamic viscosity (η) is simply given by

$$\eta = \frac{A}{\upsilon}\sigma\left(\frac{l_z}{2\pi}\right)^2 \tag{10}$$

where σ is the density of the system and υ is the resulting velocity amplitude. A careful choice of the A parameter as well as of the box edge in z-direction (see ref 35) was made in order to induce a perturbation to the system that can be discernible from thermal velocities but still small enough to prevent the appearance of order in the fluid. A rectangular box of $4 \times 4 \times 8$ nm and a value for A of 0.02 nm ps^{-2} was used. The values of υ were calculated as described in ref 35.

The values of η obtained from the simulations were 2.30×10^{-3}, 1.95×10^{-3}, and 1.52×10^{-3} kg m/s^2 at, 293 , 298, and 313 K, respectively. The experimental values[36] are 2.00×10^{-3}, 1.75×10^{-3}, and 1.22×10^{-3} kg m/s^2, at the same temperatures, respectively. The slightly higher viscosity values are consistent with the low values of the diffusion coefficient reported above.

IV. Physicochemical Properties of Water−TFE Mixtures

A. Structural Properties. Distributions of FCCO and CCOH dihedral angles do not show significant differences with those obtained in the neat fluid. The organization of the mixtures was studied using $g(r)$ of the hydrogens with respect to the TFE and water oxygens. In Figure 5 $g(r)$'s for the atom pairs O−Hw, Ow−H, O−H, and Hw−Ow, where Hw and Ow are the water hydrogen and water oxygen, respectively, are reported. The presence of a well-defined peak for the $g(r)_{\mathrm{OHw}}$ and $g(r)_{\mathrm{OwH}}$ at 0.182, and 0.165 nm, respectively, indicates the presence of a strong H-bonding interaction between the two species. The coordination numbers for the two peaks are 1.0 and 1.1, respectively. A comparative study was performed on the $g(r)_{\mathrm{OwHw}}$ and $g(r)_{\mathrm{OH}}$ to understand the interaction between the two species. For the $g(r)_{\mathrm{OwHw}}$, a first peak at 0.24 nm is observed

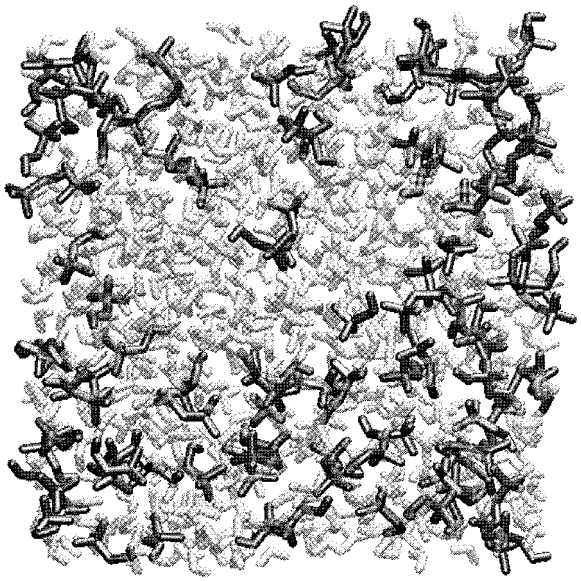

Figure 6. Snapshot of the 10 ns frame from the 34% mixture simulation. The TFE molecules are indicated by darker shading.

TABLE 6: Thermodynamic Properties of TFE−Water Mixtures[a]

%	ρ (kg/m^3)	P (bar)	ΔH_{mix} (kJ mol^{-1})	exptl ΔH_{mix} (kJ mol^{-1})
0.0	1.00	1.0	0.0	
11	1.04	0.04	0.1 (1.8)	−0.1
34	1.12	1.1	0.78 (1.1)	0.02
81	1.29	2.2	1.71 (2.0)	0.76
93	1.34	0.8	0.73 (0.8)	0.58
100	1.38	1.3	0.0	

[a] The standard deviations of the computed values are 0.01 kg/m^3 and 100 bar for density and pressure, respectively. Errors for the calculated δH_{mix} are reported in parentheses.

with a coordination number for the first shell of 0.8. In the $g(r)_{OH}$ function, a well-defined sharp peak at 0.18 nm exists with a coordination number of 0.1. In this way, it seems that the intermolecular hydrogen bonding of the TFE is mainly formed with water.

Experimental evidence based on IR and NMR studies[7] indicates the presence of strong hydrogen bonds between the two species, with TFE−water interactions replacing TFE−TFE interactions.

In Figure 6 a snapshot from the 34% mixture simulation shows clearly the microheterogeneity observed in the simulation. The figure also illustrates how the bulk of the molecules are distributed in the mixtures. It is possible to see the network of water hydrogen bonded to TFE and the clustering of CF_3 groups out of contact with the water.

B. Thermodynamic and Dynamical Properties. *Hydratation Free Energy.* The hydratation free energy was estimated using the thermodynamic integration method.[37] In this approach the Hamiltonian (H) of the system is made a function of a coupling parameter λ which when $\lambda = 0$ the system corresponds to state A and when $\lambda = 1$ the system corresponds to state B. In this way the free energy change can be calculated using

$$\Delta F_{BA} = \int_0^1 F'(\lambda)\, d\lambda = \int_0^1 \left\langle \frac{\partial H}{\partial \lambda} \right\rangle_\lambda d\lambda \qquad (11)$$

where the angular brackets $\langle\,\rangle$ denote averaging over an equilibrium ensemble generated with $H(\lambda)$. The integral in 11 was evaluated by obtaining ensemble averages over 25 discrete λ points and determining the integral numerically. At each λ point 50 ps of equilibration and 150 ps of sampling were performed. The numerical instabilities that can occur during the disappearance of atoms, were avoided using a soft-core interaction function[38,39] as described by Daura et al.[40]

The hydration free energy (ΔG_{hydr}) was calculated by deleting a TFE molecule in a box of 819 SPC water molecules. In this case the calculation was performed by switching off the nonbonded interactions between the TFE molecule and the water molecules. The simulations were performed at constant pressure and at 298 K. The value of the hydration free energy obtained was -17.9 ± 3.3 kJ mol^{-1} which is in very good agreement with the experimental value[41] of -18.02 kJ mol^{-1}.

Mixing Enthalpy. The molar enthalpy of mixing is defined as

$$\Delta H_{mix} = U_{mix} - x_{TFE}U_{TFE} - (1 - x_{TFE})U_{SPC} \qquad (12)$$

where U_{mix} is the potential energy of the mixture and U_{TFE}, x_{TFE} is the molar fraction of TFE, and U_{SPC} is the potential energy of pure TFE and pure water, respectively. In Table 6 the experimental and calculated values of the mixing enthalpy at the different concentrations of TFE are reported. Although there is considerable uncertainty in the calculations as it is dependent on the difference between large numbers, the overall trends are in good agreement with experiment.[42]

TABLE 7: Summary of Dynamical Properties of the Water−TFE Mixtures

%	D_{calc}[a]	D_{exp}[a]	ϵ_r[b]	exptl[c] ϵ_r[b]
0			62.0	78.5
4	1.44	1.13	58.7	79.9
11	1.00	0.68	57.9	75.0
34	0.76	0.65	44.2	64.8
81	0.72	0.63	28.4	31.5
93	0.97	0.64	21.5	28.0
100	0.40	0.60	17.6	26.7

[a] In 10^{-6} cm^2 s^{-1}. [b] In debyes. [c] Values taken from ref 47.

Tracer Diffusion Coefficient. Tracer diffusion coefficients for both TFE and water species have been calculated. The calculated values and the corresponding experimental data are reported in Table 7. Experimentally,[7] the diffusion coefficient of TFE in water is dependent on the concentration. The value increases slightly value at low molar ratios of TFE. This trend is also observed for other alcohols with higher values at lower concentrations of alcohol and seems correlated with the dimensions of the molecule.[43] The calculated values show the same trend but exaggerated.

The limiting value of the intradiffusion coefficient of TFE in water is about 1.13×10^6 cm^2 s^{-1}, against the calculated value of 1.44×10^6 cm^2 s^{-1}.

Dielectric Constants. A study of the dielectric properties of the water/TFE mixtures was also performed. In Table 7 the experimental and values calculated from the simulations using the same method as for the pure liquid, are reported. The calculated dielectric constant is again around 70% of the experimental value over the range of concentration studied. Considering that only the reorientational contribution to the dielectric is included, the values obtained are in reasonable agreement with the experimental ones.

V. Summary and Conclusions

We have presented a new model of TFE suitable for condensed phase simulations. The parametrization of the model was based on GROMOS96 force field with the methylene group treated as a united atom. All the calculated physicochemical properties for the pure liquid are in good agreement with the available experimental data. In the pure liquid the model shows a preference for weak local interactions between different CF_3 groups and between different OH groups. The lower than expected value of the calculated diffusion constant at 298 K could be explained by strong hydrogen-bonding interactions between the molecules. The underestimation of the dielectric constant may also be related to this, to insufficient sampling, and/or to the absence of an explicit polarization term in the force field.

The thermodynamic and dynamic properties of the water−TFE solutions are also in close agreement with the experimental data. The TFE is fully miscible with SPC water, at all molar ratios simulated. The trend in the mixing enthalpy is very close to that observed experimentally. Strong hydrogen-bonding interactions between the water and TFE together with microheterogeneity in the simulated box were observed. The microheterogeneity generated in water from the TFE molecules in the simulations is consistent with experimental SAXS studies of these mixtures.[6]

Overall, the model reproduces the experimental properties of the pure liquid and of the mixtures well. Furthermore, preliminary results of MD simulations of secondary structure

forming peptides (Betanovo and S-peptide)[44,45] in pure TFE and in mixture with SPC water have shown an increase of secondary structure with respect to the pure water simulations as expected. For these reasons, we believe that our model is suitable for use in simulation studies of peptide and protein stability and folding.

Acknowledgment. We would like to thank Berk Hess for the help for viscosity calculations and assistance with GROMACS software. We are grateful to the Deutsch Forschungsgemeinschaft (InnovationsKolleg: "Chemische Signal und biologische Antwort", Leipzig Universitat) and to the EC for the TMR projects "Fluorine as a Unique Tool for Engineering Molecular Properties" and "Structure and Dynamics of Intermediate States in Protein Folding".

References and Notes

(1) Buck, M. *Q. Rev. Biophys.* **1998**, *31* (3), 297−355.
(2) De Loof, H.; Nilsson, L.; Rigler, R. *J. Am. Chem. Soc.* **1992**, *114*, 4028−4035.
(3) van Buuren, A. R.; Berendsen, H. J. C. *Biopolymers* **1993**, *33*, 1159−1166.
(4) Bodkin, M. J.; Goodfellow, J. M. *Biopolymers* **1996**, *39*, 43−50.
(5) Biomolecular simulation: The gromos96 manual and user guide. van Gunsteren, W. F.; Billeter, S. R.; Eising, A. A.; Hünenberger, P. H.; Krüger, P.; Mark, A. E.; Scott, W. R. P.; Tironi, I. G. vdf Hochschulverlang, ETH Zürich, Switzerland, 1996.
(6) Hong, D.-P.; Hoshino, M.; Kuboi, R.; Goto, Y. *J. Am. Chem Soc.* **1999**, *121*, 8427−8433.
(7) Harris, K. R.; Newitt, P. J.; Derlacki, Z. J. *J. Chem. Soc., Faraday Trans.* **1998**, *94* (4), 1963−1970.
(8) Breneman, C. M.; Wiberg, K. B. *J. Comput. Chem.* **1990**, *11*, 361−197.
(9) Carlson, H. A.; Nguyen, T. B.; Orozco, M.; Jorgensen, W. *J. Comput. Chem.* **1993**, *14*, 1240−1249.
(10) *Gaussian 94*, revision b.3; Frisch, M. J.; Trucks, G. W.; Schlegel, H. B.; Gill, P. M. W.; Johnson, B. G.; Robb, M. A.; Cheeseman, J. R.; Keith, T.; Petersson, G. A.; Montgomery, J. A.; Raghavachari, K.; Al-Laham, M. A.; Zakrzewski, V. G.; Ortiz, J. V.; Foresman, J. B.; Peng, C. Y.; Ayala, P. Y.; Chen, W.; Wong, M. W.; Andres, J. L.; Replogle, E. S.; Gomperts, R.; Martin, R. L.; Fox, D. J.; Binkley, J. S.; Defrees, D. J.; Baker, J.; Stewart, J. P.; Head-Gordon, M.; Gonzalez, C.; Pople, J. A.; Gaussian, Inc.: Pittsburgh, PA, 1995.
(11) Xu, L.-H.; Fraser, G. T.; Lovas, F. J.; Suenram, R. D.; Gillies, C. W.; Warner, H. E.; Gillies, J. Z. *J. Chem. Phys.* **1970**, *52*, 5652−5655.
(12) Kruger, P. J.; Mettee, H. D. *Can. J. Chem.* **1963**, *42*, 340−346.
(13) Murto, J.; Rāsānen, M.; ana, T. Lotta, A. A. *J. Mol. Struct., THEOCHEM* **1984**, *108*, 99−112.
(14) Durig, J. R.; Larsen, R. A. *J. Mol. Struct.* **1989**, *238*, 195−222.
(15) Berendsen, H. J. C.; Postma, J. P. M.; DiNola, A.; Haak, J. R. *J. Chem. Phys.* **1984**, *81*, 3684−3690.
(16) Sauermann, P.; Holzapfel, K.; Oprzynski, J.; Nixdorf, J.; Kohler, F. *Fluid Phase Equilib.* **1993**, *84*, 165−182.
(17) Berendsen, H. J. C.; Grigera, J. R.; Straatsma, T. P. *J. Phys. Chem.* **1987**, *91*, 6269−6271.
(18) Hess, B.; Bekker, H.; Berendsen, H. J. C.; Fraaije, J. G. E. M. *J. Comput. Chem.* **1997**, *18*, 1463−1472.
(19) Miyamoto, S.; Kollman, P. A. *J. Comput. Chem.* **1992**, *13*, 952−962.
(20) Allen, M. P.; Tildesley, D. J. *Computer Simulations of Liquids*; Oxford Science Publications: Oxford, UK, 1987.
(21) Morishita, T. *J. Chem. Phys.* **2000**, *113*, 2976−2982.
(22) Straatsma, T. P.; Berendsen, H. J. C.; Stam, A. J. *Mol. Phys.* **1986**, *57*, 89.
(23) Berendsen, H. J. C.; van der Spoel, D.; van Drunen, R. *Comput. Phys. Comm.* **1995**, *91*, 43−56.
(24) Curtiss, L. A.; Frurip, D. J.; Blander, M. *J. Am. Chem. Soc.* **1978**, *100*, 79−86.
(25) Radnai, T.; Ishiguro, S.; Ohtaki, H. *J. Solution Chem.* **1989**, *18*, 771−784.
(26) Rochester, C. H.; Symonds, J. R. *J. Chem. Soc., Faraday Trans. 1* **1973**, 1267−1273.
(27) Walser, R.; Mark, A. E.; van Gunsteren, W. F. *J. Chem. Phys.* **1999**.
(28) Herzberg, G. *Molecular Spectra and Molecular Structure. II. Infrared and Raman Spectra of Polyatomic Molecules*; Van Nostrand Reinhold Co.: New York, 1945.
(29) Perttilä, M. *Spectrochim. Acta* **1979**, *35A*, 585−592.
(30) Kalasinsky, V. F.; Anjaria, H. V. *J. Phys. Chem.* **1980**, *84*, 1940−1944.
(31) Miyanaga, S.; Tamura, K.; Murakami, S. *J. Chem. Thermdyn.* **1992**, *24*, 291−296.
(32) Neumann, M. *Mol. Phys.* **1983**, *50*, 841.
(33) Madelung, O. *Landolt-Bornstein: Static Dielectric Constants of Pure Liquids and Binary Liquid Mixtures*; Vol. New Series IV/6. Springer-Verlag: Berlin, Germany, 1976.
(34) Berendsen, H. J. C. In *Computer Simulations in Material Science*; Meyer, M., Pontikis, V., Eds.; Kluwer: Dordrecht, 1991; pp 139−155.
(35) Feenstra, K. A.; Hess, B.; Berendsen, H. J. C. *J. Comput. Chem.* **1999**, *20*, 786−798.
(36) Riddick, J. A.; Burger, W. B.; Sakano, T. K. O*rganic Solvents*, 4th ed.*;* Wiley-Interscience: New York, 1986.
(37) Mark, A. E. In *Encyclopaedia of Computational Chemistry 2*; von Rague Schleyer, P., Ed.; John Wiley & Sons: New York, 1998; pp 1211−1216.
(38) Beutler, T. C.; Mark, A. E.; van Schaik, R. C.; Gerber, P. R.; van Gunsteren, W. F. *Chem. Phys. Lett.* **1994**, *222*, 1994.
(39) Zacharias, M.; Straatsma, T. P.; McCammon, J. A. *J. Chem. Phys.* **1994**, *100*, 9025.
(40) Daura, X.; Hünenberger, P. H.; Mark, A. E.; Querol, E.; Aviles, F. X.; van Gunsteren, W. F. *J. Am. Chem. Soc.* **1996**, *118*, 6285.
(41) Cabani, S.; Gianni, P.; Mollica, V.; Lepori, L. *J. Solution Chem.* **1981**, *10*, 563−595.
(42) Cooney, A.; Marcom, K. W. *J. Chem. Thermodyn.* **1988**, *20*, 735−741.
(43) Mills, R. *J. Phys. Chem.* **1973**, *77*, 685.
(44) Kortemme, T.; Ramirez-Alvarado, M.; Serrano, L. *Science* **1998**, *281*, 253−256.
(45) Nelson, J. W.; Kallenbach, N. R. *PROTEINS: Struct. Funct. Gen.* **1986**, *1*, 211−217.
(46) Cooney, A.; Marcom, K. W. *J. Chem. Thermodyn.* **1988**, *20*, 1469−1476.
(47) Rochester, C. H.; Symonds, J. R. *J. Chem. Soc., Faraday Trans. 1* **1973**, 1274−1281.